Compton-scattering study of the electronic properties of the transition-metal alloys FeAl, CoAl, and NiAl

S. Manninen, V. Honkimäki, K. Hämäläinen, and J. Laukkanen
Department of Physics, P.O. Box 9, FIN-00014 University of Helsinki, Helsinki, Finland

C. Blaas and J. Redinger
Institut für Technische Elektrochemie, Technische Universität Wien, Getreidemarkt 9/158, A-1060 Wien, Austria

J. McCarthy and P. Suortti
European Synchrotron Radiation Facility, Boîte Postale 220, F-38043 Grenoble, France
(Received 7 September 1995)

Directional Compton profiles of the transition-metal alloys FeAl, CoAl, and NiAl have been measured. Both a conventional technique (resolution 0.55 a.u. of momentum), based on a 59.3-keV x-ray source with a solid-state detector, and a high-resolution spectrometer (0.15 a.u. of momentum) with 50-keV x rays from a synchrotron source have been used. The results are interpreted using a theory based on a full-potential linearized augmented-plane-wave method. The agreement between the experimental and the theoretical momentum density anisotropy is very good. It is shown that the anisotropies at low momenta are heavily influenced by the particular shape of the Fermi surface.

I. INTRODUCTION

The first period transition metals form interesting alloys with aluminum covering the entire concentration range. The equiatomic alloys of Fe, Co, and Ni crystallize in a simple CsCl-type crystal structure.[1] A great effort has been made to study the character of the bonding and the charge transfer in these alloys. Charge density studies, based on x-ray diffraction, and both soft x-ray and electron spectroscopy have been used. Depending on the experimental method and the definition of the charge transfer the results are quite diffuse and even conflicting.[2]

Compton-scattering experiments using polycrystalline samples have been made by Chaddah and Sahni[3] who measured FeAl and CoAl and by Manninen *et al.*[2] who measured FeAl, CoAl, and NiAl, using a γ-ray source and a solid-state detector. The analysis was mostly based on the charge transfer and on a rigid band model where the transfer took place between the valence electron states of aluminum and 3*d* states of the transition metal. The general trend turned out to be a net transfer to the transition metal site. Because polycrystalline samples were used, a detailed analysis of the directional electron momentum distribution itself was not possible.

Podloucky and Neckel[4] calculated the directional Compton profiles of FeAl using a quasi-self-consistent augmented plane wave (APW) method. They found a remarkable anisotropy that should easily be seen even in a low-resolution experiment. Unfortunately no single crystals were available at that time. Later the Vienna group developed their method by introducing a multipole expansion of the momentum density to calculate the Compton profile and by including a modern version of linearized APW.[5] They calculated the directional FeAl profiles and compared those with the first test experiments on single crystals.[6] Due to the low resolution, only some gross features of the anisotropy could be compared.

In this work we present high-resolution data on the directional Compton profiles of FeAl, CoAl, and NiAl single crystals. Our experiments are made using the focusing scanning spectrometer at the High Energy Beam line (ID15) at the European Synchrotron Radiation Facility (ESRF). The average resolution in the momentum range of interest is about 0.15 a.u. For comparison and also to check the consistency of data processing, all crystals have also been measured using the conventional spectrometer at the University of Helsinki, which is based on the use of monochromatic W $K\alpha_1$ x rays and a solid-state detector.

The theoretical analysis is based on a full potential linearized augmented plane wave (FLAPW) method. Special attention is taken to separate the wave function and the Fermi surface contributions to the momentum anisotropy. The results will demonstrate the usefulness of Compton scattering in the Fermiology of imperfect single crystals at room temperature.

II. THEORY

Within the impulse approximation[7,8] the Compton profile (CP) is the projection of the electron momentum density (EMD) onto the scattering vector. A practical method for the calculation of CP's for cubic systems representing both EMD and CP's in terms of multipole expansions was described by Blaas *et al.*[5] Within this scheme, the EMD coefficients are obtained by a Gaussian projection from EMD calculated on a set of special directions. The corresponding CP coefficients are computed by a one-dimensional integration involving the EMD coefficients.

The self-consistent charge densities of FeAl, CoAl, and NiAl at the proper experimental lattice constants *a* were determined by means of the all-electron FLAPW method,[9] which solves the Kohn-Sham type Schrödinger equation without any shape restrictions of the crystal potential. The

TABLE I. Parameters for the valence CP calculations. [a = lattice constant, p_{max} = maximum momentum value for anisotropies, P_{max} = maximum momentum value for the isotropic cutoff correction, $N(p_{max})$ = norm of the valence EMD inside momenta $\leq p_{max}$, $N(P_{max})$ = norm of the valence EMD inside momenta $\leq P_{max}$ = norm of the valence CP for momenta $\leq P_{max}$.]

	FeAl	CoAl	NiAl
a (a.u.)	5.49619	5.40907	5.45450
p_{max} (a.u.)	7.43	7.55	7.49
P_{max} (a.u.)	41.15	41.82	41.47
$N(p_{max})$	10.753	11.672	12.523
$N(P_{max})$	10.999	12.000	12.997

exchange and the correlation were treated within the local density approximation (LDA). The self-consistency iterations have been performed on a 97-point linear tetrahedron grid within the irreducible wedge of the first Brillouin zone. About 3000 warping terms in the interstitial region and nonspherical contributions up to $l=12$ inside the muffin-tin spheres have been used for the representation of the general potential and about 200 FLAPW's for the variational basis set.

The valence EMD at any given momentum value can be obtained by a straightforward Fourier inversion of the FLAPW wave functions and the subsequent squaring. In order to determine the EMD expansion coefficients the EMD was computed using a momentum interval of $0.01(2\pi/a)$ with a maximum momentum value of $6.5(2\pi/a)$ along each of the 45 special directions[10,11] determining the expansion coefficients up to $l=48$ (in total 29 250 EMD values). Beyond $6.5(2\pi/a)$ only the isotropic part was considered, which is enough to ensure the correct norms of the valence EMD (CP's). The relevant parameters for the valence calculations can be found in Table I. The total CP's were calculated by adding an atomiclike core contribution and a Lam-Platzman term[12] that corrects for the electron correlation effects beyond the noninteracting jellium model limit (isotropic in the case of the LDA).

III. EXPERIMENT

The single crystals used in this work were grown by the Bridgman method at the University of Lausanne. Slices, all with the same thickness of 2 mm and a diameter of at least 20 mm, were cut using the electroerosion technique. The orientation of each sample was verified using Laue diffraction so that the Bragg planes were parallel to the crystal surface. It turned out that the CoAl crystals were not uniform single crystals but grains big enough for the experiment were present. In the case of FeAl the Laue spots were slightly diffused, indicating a small deviation from an ideal single crystal. However, this mosaicity was less than the angular resolution of the Compton spectrometer. All orientations were correct within $\pm 1°$.

Preliminary experiments were done using an x-ray spectrometer based on the use of monochromatic W $K\alpha_1$ radiation and a solid state detector.[13] The small beam size (0.5 mm horizontal, 10 mm vertical) allowed the use of small single-crystal volumes of the CoAl samples. The resolution

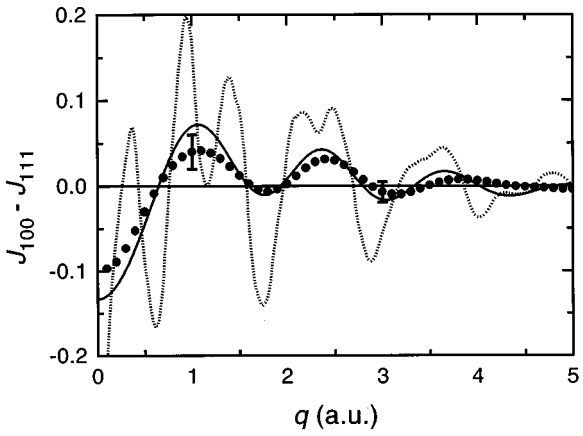

FIG. 1. The Compton profile anisotropy [100]–[111] of FeAl. The experimental result (solid dots) has been obtained using W $K\alpha_1$ radiation and a solid-state detector (resolution about 0.55 a.u.). The dotted line corresponds to the FLAPW theory and the solid line to the theory convoluted with the resolution function.

of this spectrometer was about 0.55 a.u. of momentum fully dominated by the poor energy resolution of the solid-state detector. The scattering angle was 160° and altogether about 10^7 counts were collected for each direction. The data were corrected for the background, instrumental broadening [because of the statistical noise, this can be done only partly, the residual instrument function (RIF) should be known], and absorption in the sample and then converted into the momentum scale. The contribution of multiple scattering was calculated using a Monte Carlo method.[14] This was about 11% in each case. The areas of the experimental profiles were normalized to the number equal to the single+multiple scattering contribution (the single scattering contribution equals the number of electrons). The directional difference profiles were then compared with the theory, which should be convoluted by the RIF. When the difference is taken, most of the possible small systematic errors cancel out.

The comparison between the experimental and the theoretical Compton profile differences J_{100}-J_{111} is shown in Fig. 1 for FeAl. It is clearly seen that the experimental result is very close to the theoretical one after the convolution but the details predicted by the theory are totally washed out due to the low resolution. Similar results were also obtained in the case of CoAl and NiAl. It will be shown in Sec. IV that these details are mainly due to the Fermi-surface effects and it is obvious that better resolution is required in order to find those experimentally. On the other hand, when insulating systems (like ionic crystals) are studied this resolution is good enough to see all the essential gross features in the momentum anisotropy.[15]

The high-resolution spectrometer located at the ESRF beam line BL25 (ID15) was used for the final experiment. A schematic layout of the experimental arrangement is shown in Fig. 2. Radiation from the multipole asymmetric wiggler (7 periods, critical energy 43 keV) was monochromatized using a horizontally focusing Bragg type bent Si(220) crystal. A photon energy of 49.6 keV was chosen and the energy bandwidth of the focused beam at the sample was about 15 eV. The beam was slitted down to 0.15 mm(horizontal)×6 mm(vertical) and the scattering angle was 161°. The scat-

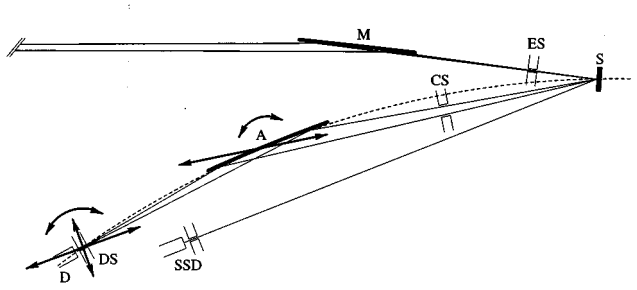

FIG. 2. A schematic layout of the ESRF spectrometer. The monochromatized beam (M) is collimated before the sample (S) by the aperture slits (ES) and the scattered beam is collimated before the analyzer (A) by the aperture slits (CS). The sample, analyzer crystal, and detector slits (DS) are on the Rowland circle (dashed line), which has a constant radius but whose position is moving during the scan around the sample position. A NaI scintillation counter was used as a detector (D) and a Ge solid-state detector (SSD) as a monitor. The translations and rotations of the analyzer crystal and the detector are indicated by arrows. The monochromator part is scaled down by a factor of 100 and the spectrometer part is scaled down by a factor of 10.

tered energy spectrum was analyzed using a bent focusing Ge(440) crystal (80×61 mm^2, bending radius 6100 mm) in a scanning mode, followed by a NaI(Tl) scintillation counter moving simultaneously with the analyzing crystal. With the synchronous motions, the sample, analyzer, and detector stay on the focusing circle during the scan. In this type of spectrometer, the crucial factor limiting the resolution is the size of the irradiated sample volume seen by the analyzer crystal.

The resolution function was calculated as a function of energy. The resolution is affected by the horizontal and the vertical beam divergences, the absorption effect to the horizontal divergence, the reflectivities of the monochromator and the analyzing crystals, and the Johann error of the bent crystal. The resulting resolution function was very close to a Gaussian with the full width at half maximum of 165 eV at the elastic line (49.6 keV) and 126 eV, 94 eV and 72 eV at the high-energy side of the experimental Compton profile (45.7 keV), at the peak center (41.7 keV) and at the low-energy side (38.4 keV), respectively. In terms of the momentum resolution this corresponds to 0.15 a.u. at the Compton peak, good enough to see the details predicted by the theory.

To check the resolution function calculation a fluorescence spectrum of the Gd sample was measured. The $K\alpha_1$ fluorescence line (43 keV) is close to the center of the Compton peak and the absorption of Gd is also similar to the actual samples, giving roughly the same irradiated volume. Including the natural linewidth of the fluorescence line (26 eV) and the effects that are different for the fluorescence and scattered radiation (the effect of primary energy distribution) the calculated and the measured resolution functions were identical within the statistical error.

The experimental procedure for each sample was first to measure one full spectrum covering the whole energy range from the elastic line to the low-energy tail of the Compton profile using a time step of 10 s and an angular step of 0.01° of the analyzing crystal. The actual Compton profile (from 38.4 to 45.7 keV) was then measured with an angular step of 0.005°, corresponding to an energy step of 24 eV at the

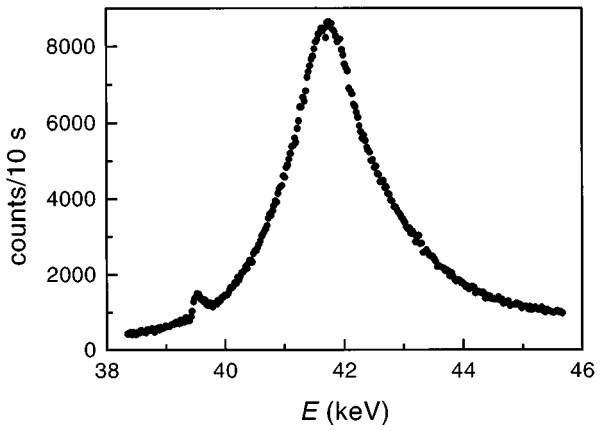

FIG. 3. The experimental Compton profile (raw data) of FeAl [111] taken during 1 h. The small extra peak at 39.5 keV corresponds to the elastic line, seen by the Ge(551) reflection of the analyzer crystal (see text).

Compton peak. Such a measurement took about 1 h and total of two full 8-h shifts were used for each crystal direction. The counting rate was about 1000 counts/s at the Compton peak and total of 1.5×10^7 counts were collected for each sample.

A monitor counter, measuring the Compton scattering from the sample with a Ge detector, was used to correct for the fluctuations of the primary beam intensity. It also turned out that there were additional contributions to the measured spectra due to the Compton scattering of the monochromator Si(440) harmonic seen by the Ge(660) reflection of the analyzer crystal and the elastic line seen by the Ge(551) reflection. This can be seen in Fig. 3, which shows the raw data for FeAl(111) crystal. Fortunately, this did not overlap with the interesting part of the spectra.

The measured spectra were first normalized according to the monitor count rate. The background contribution was subtracted using a polynomial fit. The energy-dependent corrections to the measured cross section are considerably more complicated than in the case of conventional energy dispersive measurement with a solid-state detector. By assuming a linear polarization for the white beam from the wiggler, the polarization factors were properly included in the calculations for the monochromator, sample, and the analyzing crystal. The measured data were corrected for air and sample absorption and the geometrical factors due to the vertical and horizontal opening angles. The reflectivity of the analyzing crystal was also taken into account. Data points, so far in the angular scale, were then converted to the momentum scale including the differential element correction due to the nonlinear transformation. Finally the experimental profiles were normalized within the range of ± 6 a.u. to the theoretical values. No correction for the multiple scattering was done. The major part of this smooth contribution was subtracted together with the background. The sample thicknesses and volumes were about the same and when the directional differences are taken, there are only residual effects remaining. It turns out that the multiple scattering contribution is in general smaller in the synchrotron radiation experiments[16] compared with the experiments using an unpolarized source. Also, the focusing optics naturally limits the multiple-

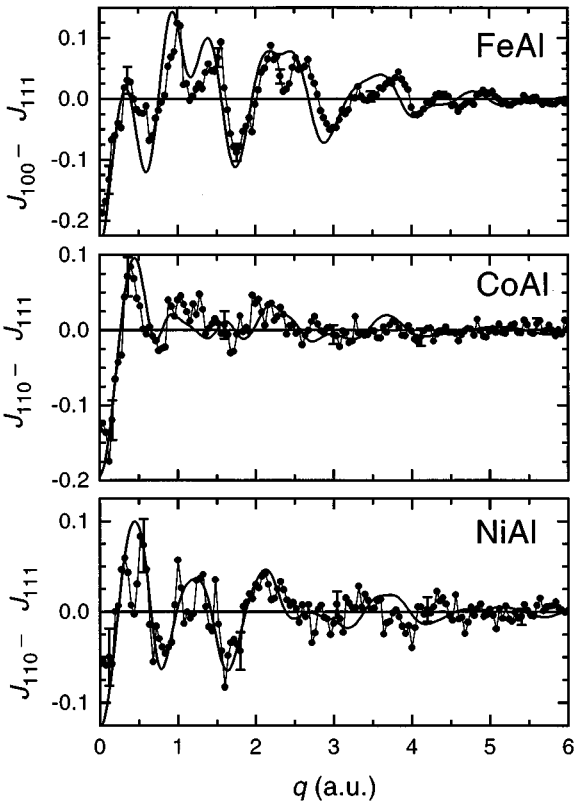

FIG. 4. The experimental and theoretical directional difference profiles of FeAl ([100]–[111]), CoAl ([110]–[111]), and NiAl ([110]–[111]). The solid line corresponds to the FLAPW theory convoluted with the experimental resolution function and the solid circles connected with a thin line are the experimental data points. The statistical error bars are shown at some points.

scattering contribution because the analyzing crystal accepts photons only from a very small sample volume. In the present case this means that the multiple-single ratio of about 11% for a conventional x-ray source is now less than 10% and the major part of it is removed in the subtraction of the background. The remaining contribution in the directional Compton profile difference curves is therefore smaller than the statistical error.

IV. RESULTS AND DISCUSSION

The final experimental Compton profile anisotropies are given in Fig. 4 for FeAl, CoAl, and NiAl. The average of both sides of the experimental Compton profile is used excluding the Bragg reflection region around 39.5 keV (discussed before and shown in Fig. 3). Together with the experimental anisotropies the theoretical results after the convolution with the experimental resolution function are also shown. Although the statistical accuracy is somewhat limited, some general conclusions can be drawn. The gross features, as seen with lower resolution in Fig. 1 for FeAl are now replaced by fine structure especially at low momenta. In the case of CoAl these low momentum details are actually all that can be clearly separated from the statistical noise. At high momenta where almost all information comes from the tightly bound atomiclike electrons, all experimental difference curves approach zero. This gives confidence that the remaining uncertainties in the final experimental results mainly cancel out when the difference is taken.

A main motivation for developing high-resolution Compton scattering was the prospect to tackle the Fermiology aspects of the electronic structure. From the figures above we conclude that the experimental resolution reached so far is already good enough to reproduce the fine structures predicted by theory (compare Figs. 1 and 4). It is therefore necessary to get a clear picture of the physics behind the maxima and minima in the difference Compton profiles (DCP's) and to attribute them, if possible, either to wave-function-related effects or to the topology of the Fermi surface.

Despite their different lattice constants, the band structures of the three compounds are remarkably similar (see, e.g., Refs. 17 and 18 and confirmed by the present work) exhibiting an almost rigid-band-like behavior upon increasing the number of valence electrons in the series FeAl, CoAl, NiAl. However, the shape of the Fermi surface is different, since the Fermi level for FeAl is well within the d-band complex, for CoAl just below the upper d-band edge, and for NiAl well above the d bands. The contributions to the Fermi surface come from the fourth, fifth, and sixth bands for FeAl and from the sixth and seventh bands for both CoAl and NiAl. Roughly speaking, in FeAl the fourth and fifth bands cut out holes around Γ and R points, while the sixth band adds electrons except for tubes along Γ-X and regions around R points (see Fig. 5). For CoAl and NiAl the sixth band is almost full, leaving only the holes around the R points. The seventh band progressively adds electrons around M points.

In theory it is possible to remove all Fermi-surface-related features from the present FLAPW EMD by artificially filling 7 bands (14 electrons), which means that for all three compounds the d bands are filled as well as one plane-wave-like state below and one above the d-band complex (see, e.g., Ref. 18). Scaling momentum values to units of the lattice constants $(2\pi/a)$ one ends up with model EMD's that are very similar for all three alloys, thus confirming the rigid-band-like behavior. The remaining differences between the individual model EMD's are small and mainly isotropic, reflecting the narrowing of the d bands (NiAl $<$ CoAl $<$ FeAl) whereas the anisotropic parts are almost identical.

In Fig. 6 the theoretical DCP's involving the main symmetry directions are shown both for the real alloys and for the model alloys with 7 completely filled bands. The model DCP's for all three alloys agree with each other extremely well, whereas the different shapes of the Fermi surfaces introduce characteristic changes. In other words, these changes are caused by removing the excess momentum density from regions outside the Fermi surfaces. The most pronounced effects can be found in the low momenta regions. The changes are largest for FeAl, especially if the [100] direction is involved,[19] which is hardly surprising since the Fermi surface cuts right through the Fe d bands. For NiAl, which already has an almost filled d band, the Fermi-surface-induced changes are large only for $q<1(2\pi/a)$. For larger momenta the changes are small and the anisotropies are attributed mainly to the wave-function-related e_g/t_{2g} splitting of the Ni d bands.

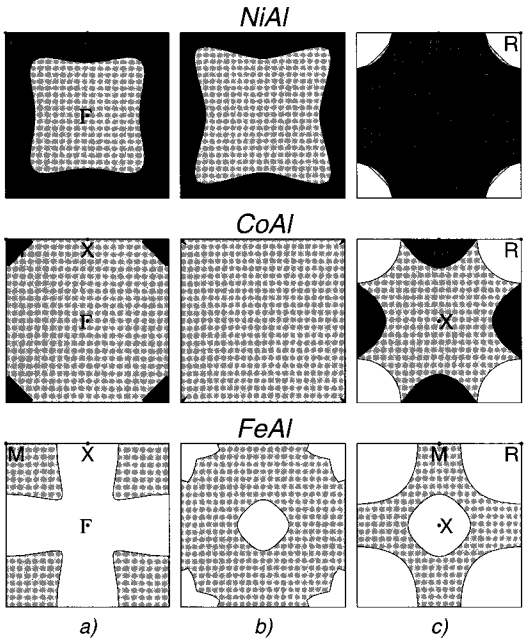

FIG. 5. Intersections of the Fermi surfaces of FeAl, CoAl, and NiAl with planes perpendicular to [100] at various distances q from the origin. Occupied areas for the sixth band sheet are shaded light grey, those for the seventh band sheet dark grey (the sixth band has to be occupied in regions occupied by the seventh band): (a) $q=0$, 1, 2, 3 $(2\pi/a),\ldots,$ (b) $q=0.2, 0.8, 1.2, 1.8, 2.2, 2.8, 3.2$ $(2\pi/a),\ldots,$ (c) $q=0.5, 1.5, 2.5$ $(2\pi/a),\ldots$ The labels Γ, R, M, X indicate the high-symmetry points of the simple-cubic Brillouin zone.

In the following we examine the Fermi-surface-induced changes for low momenta using the DCP [110]−[111] as an example. Out of the three alloys NiAl is certainly best suited for such considerations since its Fermi surface cuts mainly through the upper plane-wave-like band number 7. In a simple plane-wave approach, neglecting the almost filled Ni d bands for the moment, a fully occupied lower and upper plane-wave-like band (4 electrons) fills 2 simple cubic Brillouin zones, i.e., one rhombic dodecahedron, completely. This rhombic dodecahedron repeated periodically throughout momentum space (dodecahedra model) describes artificial NiAl without Fermi surface. In order to represent true NiAl with a Fermi surface (3 plane-wave-like electrons) the actually filled fraction of momentum space may be approximated by a sphere inscribed into each of the rhombic dodecahedra (spheres model, for the correct Fermi surface of NiAl see Fig. 5).[20] The implications of the plane-wave approach are illustrated in Fig. 7. Since the EMD drops off rapidly outside the central rhombic dodecahedron it is sufficient to concentrate on the momentum region inside its circumscribed sphere of radius $1(2\pi/a)$ as indicated in the figure. (Note that the plane-wave d hybridization pushes about 5% of the plane-wave-like electrons from the central rhombic dodecahedron into adjacent rhombic dodecahedra. For simplicity we will assume a constant momentum density within each rhombic dodecahedron.) For the dodecahedra model (NiAl without Fermi surface) the DCP is proportional to the difference between the (direction dependent) cross sections of the rhombic dodecahedra viewed along the two directions. Comparing the planes of integration perpendicular to the two directions at $q=0$ we see that the area of the cross section of the central rhombic dodecahedron viewed along [110] is larger than that viewed along [111]. As the EMD within the neighboring rhombic dodecahedra is already much lower, their contributions are too small to change the trend imposed by the central rhombic dodecahedron. Consequently, the DCP [110]−[111] (Fig. 6) for completely filled bands is positive at $q=0$. For the spheres model (NiAl with Fermi surface) we have to look at the cross sections of the Fermi spheres inscribed into each of the space-filling rhombic dodecahedra. The cross sections of the Fermi sphere inside the central rhombic dodecahedron are identical for all directions. However, viewed along [111] there are contributions from six Fermi spheres inside adjacent neighboring rhombic dodecahedra as opposed to only two when viewed along [110]. Therefore, the DCP [110]−[111] (Fig. 6) for the physical alloy is negative at $q=0$. Invoking similar argu-

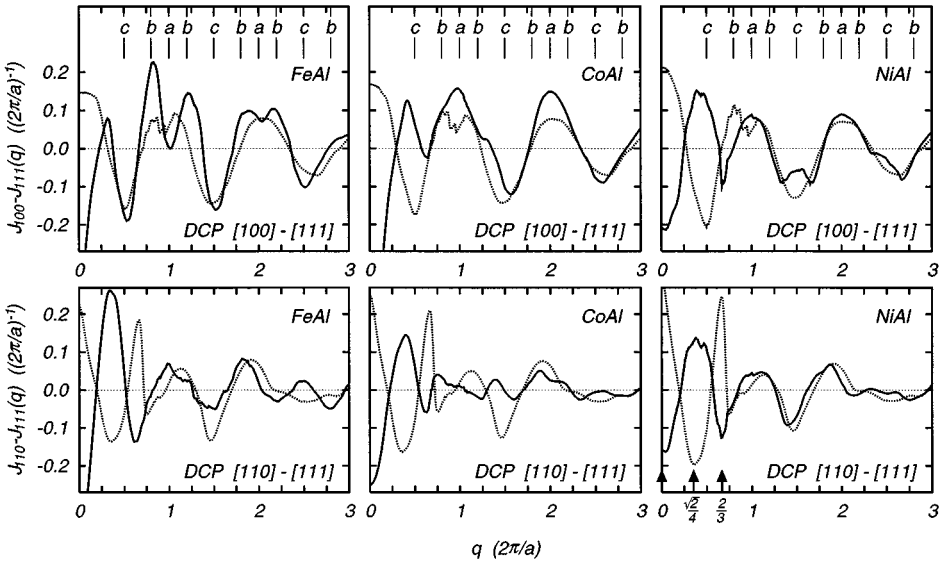

FIG. 6. Theoretical difference Compton profiles [100]−[111] (upper panel) and [110]−[111] (lower panel) for FeAl, CoAl, and NiAl. The solid lines represent the physical alloys while the dotted lines are the corresponding systems with artificially filled 7 bands (see text). The labels a, b, c mark q values for which the Fermi-surface cross sections involved in the computation of the Compton profiles along [100] are shown in Fig. 5.

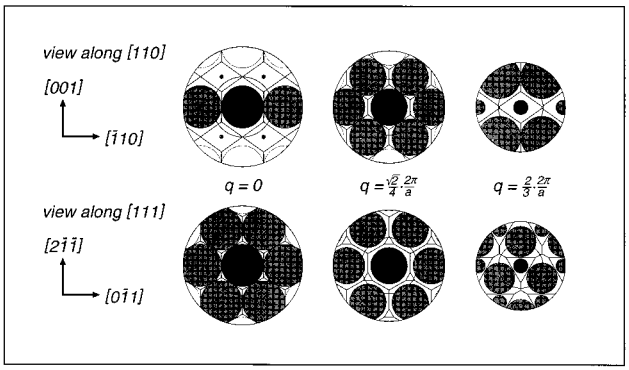

FIG. 7. Illustration of a simple plane-wave approach for NiAl. The upper part shows, for selected q values, the planes of integration used in computing the Compton profile along [110], the lower part those for the Compton profile along [111]. In Fig. 6 these q values are marked by arrows. The cross sections of space-filling rhombic dodecahedra with each plane are indicated by straight lines (dodecahedra model, NiAl without Fermi surface). The shaded areas represent the actually occupied momentum regions for NiAl with a Fermi surface (spheres model) and the grey level indicates the magnitude of the electron momentum density. Hence, the contribution from the Fermi sphere centered at the origin is colored dark grey, those from the nearest neighbors of type $\langle 110 \rangle$ medium grey, and all higher contributions light grey. The inner sphere that circumscribes the central rhombic dodecahedron has a radius of $1(2\pi/a)$ and the outer circle corresponds to a momentum sphere of radius $2(2\pi/a)$.

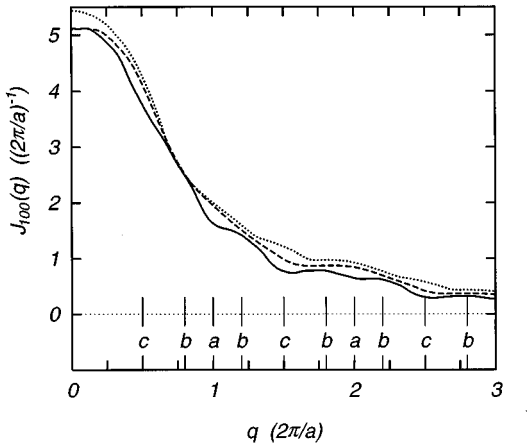

FIG. 8. Theoretical valence Compton profiles along [100] for FeAl (solid), CoAl (dashed), and NiAl (dotted). The labels a, b, c mark q values for which the Fermi-surface cross sections involved in the computation of the Compton profiles are shown in Fig. 5.

ments at $q=\sqrt{2}/4(2\pi/a)$ and $q=2/3(2\pi/a)$ we are able to explain the Fermi-surface-induced reversal of sign in the DCP [110]−[111] (Fig. 6). However, it should be noted that for $q>1(2\pi/a)$ the plane-wave-like bands no longer contribute to the CP anisotropies significantly and hence any anisotropy in this region has to be attributed to the transition-metal d bands.

While the Fermi-surface-induced changes for $q<0.8(2\pi/a)$ show a similar trend for all three alloys in the DCP [110]−[111], the picture changes if the [100] direction is involved as can be seen in Fig. 6. While NiAl due to the almost filled d bands shows again the same pattern concerning the deviation from the 7 filled bands model, FeAl shows a remarkable double-peak structure around $q=1(2\pi/a)$, displaying an additional minimum. Also the anisotropies for $q>1(2\pi/a)$ are more pronounced in the DCP's [100] −[111]. Therefore, taking a closer look at the [100] valence CP's, shown in Fig. 8, is appropriate. Due to the increasing number of valence electrons one expects that CP(FeAl) <CP(CoAl)<CP(NiAl) for all q values. Apparently the CP's for CoAl and NiAl are smoother than for FeAl. CoAl and NiAl have an almost filled sixth band, whereas for FeAl the sixth band Fermi surface additionally has tubular holes along Γ-X (see Fig. 5). Using geometrical arguments one sees that the cross section through the occupied part of the sixth band in FeAl (Fig. 5) is largest for the q values labeled (b), leading to distinct bumps in the CP [100] of FeAl at these q values [again labeled (b) in Fig. 8]. The fourth and fifth band Fermi surfaces of FeAl (not shown in Fig. 5) support the trend given by the sixth band. The bumps in the CP [100] of FeAl (caused by the particular Fermi-surface shape) have been identified to be responsible for the double-peak structure in the DCP [100]−[111] of FeAl.[19] The seventh band, unoccupied in FeAl, contributes to the CP [100] for CoAl and NiAl and the shape of its Fermi surface is again responsible for the size of the contribution. From Fig. 5 one sees that for q values labeled (b) the seventh band Fermi surface cross section is minimal for NiAl and practically nonexistent for CoAl. Consequently, at these q values [labeled (b) in Fig. 8] the CP's for the three alloys are closer to each other than for any other value of q. At q values labeled (c) the seventh band is almost completely occupied for NiAl leading to bumps in the CP [100] at those q values. This is in contrast to CoAl, which has a smaller cross section at those q values, which explains why the differences between the CP's of CoAl and NiAl are larger for q values labeled (c) (corresponding to cuts along the Brillouin zone boundaries) than for those labeled (a) (corresponding to cuts through the Brillouin zone centers). These facts together with the analysis presented above demonstrate that the transition-metal aluminides are well suited for studying their Fermiology by high-resolution Compton scattering since the wave-function-related differences between these three alloys are small whereas the Fermi-surface-related differences are large.

V. SUMMARY

Based on the high-resolution Compton scattering experiment combined with the state-of-the-art band-structure analysis we have shown that the effect of the Fermi surface can be clearly seen in the directional difference Compton profiles. Because low temperature and high single crystal quality are not required we suggest that this type of experiment opens up new possibilities in the Fermiology studies of even more complex systems. The relatively low statistical accuracy, limiting the full potential of the analysis at the moment will not be the problem when the improved version of the ESRF spectrometer will be in the operational stage.

ACKNOWLEDGMENTS

We wish to thank Professor S. G. Steinemann, University Lausanne/Switzerland, for providing the samples and Dr. P. Marksteiner, University Vienna computing center, for his kind help in determining the Gaussian directions. The present work was supported by the Academy of Finland (Contract No. 8582). One of the authors (C.B.) would like to acknowledge the financial support from the International Center for Computational Materials Science in Vienna.

[1] D. Singh, in *Intermetallic Compounds: Vol. 1, Principles*, edited by J. H. Westbrook and R. L. Fleischer (Wiley, New York, 1994), pp. 127–147, and references therein.

[2] S. Manninen, B. K. Sharma, T. Paakkari, S. Rundqvist, and M. W. Richardsson, Phys. Status Solidi B **107**, 749 (1981).

[3] P. Chaddah and V. C. Sahni, Philos. Mag. B **37**, 305 (1978).

[4] R. Podloucky and A. Neckel, Phys. Status Solidi B **95**, 541 (1979).

[5] C. Blaas, J. Redinger, R. Podloucky, P. Jonas, and P. Schattschneider, Z. Naturforsch. **48a**, 198 (1993).

[6] S. Manninen (private communication).

[7] P. M. Platzman and N. Tzoar, Phys. Rev. **139**, A410 (1965).

[8] P. Eisenberger and P. M. Platzman, Phys. Rev. A **2**, 415 (1970).

[9] H. J. F. Jansen and A. J. Freeman, Phys. Rev. B **30**, 561 (1984).

[10] W. R. Fehlner and S. H. Vosko, Can. J. Phys. **54**, 2159 (1976).

[11] P. Marksteiner (private communication).

[12] L. Lam and P. M. Platzman, Phys. Rev. B **9**, 5122 (1974).

[13] S. Manninen, V. Honkimäki, and P. Suortti, J. Appl. Crystallogr. **25**, 268 (1992).

[14] V. Halonen, B. G. Williams, and T. Paakkari, Phys. Fenn. **10**, 107 (1975).

[15] J. Redinger, R. Podloucky, S. Manninen, T. Pitkänen, and O. Aikala, Acta Crystllogr. Sec. A **45**, 478 (1989).

[16] F. Bell and J. Felsteiner, Nucl. Instrum. Methods Phys. Res. Sect. B **101**, 379 (1995).

[17] K. Pechter, P. Rastl, A. Neckel, R. Eibler, and K. Schwarz, Monatsh. Chem. **112**, 317 (1981).

[18] R. Eibler and A. Neckel, J. Phys. F **10**, 2179 (1980).

[19] C. Blaas, J. Redinger, S. Manninen, V. Honkimäki, K. Hämäläinen, and P. Suortti, Phys. Rev. Lett. **75**, 1984 (1995).

[20] The plane-wave approach for NiAl is justified by an H-NFE-TB (hybridized–nearly-free-electron–tight-binding) analysis of the first-principles band structure (Ref. 18). The H-NFE-TB analysis shows that switching on the plane-wave *d* hybridization increases the number of plane-wave-like electrons from 3.00 to 3.56. 1.93 plane-wave-like electrons are of type $\langle 000 \rangle$ and 1.48 of type $\langle 100 \rangle$, which populate the Fermi volume inside the rhombic dodecahedron centered at the origin (000). Only 0.15 plane-wave-like electrons are of types $\langle 110 \rangle$ and $\langle 111 \rangle$, which populate the Fermi volumes inside the rhombic dodecahedra centered at positions {110}. Completing all 7 bands adds electrons mainly of type $\langle 100 \rangle$ filling the central rhombic dodecahedron completely.